Thermodynamics and phase structure of an Einstein-Maxwell-scalar model in extended phase space

Guangzhou Guo,[*] Peng Wang,[†] Houwen Wu,[‡] and Haitang Yang[§]
Center for Theoretical Physics, College of Physics, Sichuan University, Chengdu 610064, China

(Received 27 July 2021; accepted 17 March 2022; published 30 March 2022)

In this paper, we study thermodynamics and phase structure of asymptotically AdS hairy and Reissner-Nordström-AdS (RNAdS) black holes in the extended phase space, where the cosmological constant is interpreted as a thermal pressure. The RNAdS and hairy black holes are black hole solutions of an Einstein-Maxwell-scalar (EMS) model with a nonminimal coupling between the scalar and electromagnetic fields. The Smarr relation, the first law of thermodynamics and the free energy are derived for black hole solutions in the EMS model. Moreover, the phase structure of the RNAdS and hairy black holes is investigated in canonical and grand canonical ensembles. Interestingly, RNAdS BH/hairy BH/RNAdS BH reentrant phase transitions, consisting of zeroth-order and second-order phase transitions, are found in both ensembles.

DOI: 10.1103/PhysRevD.105.064069

I. INTRODUCTION

The first observations of gravitational waves by LIGO [1] and the first image of a black hole in the galaxy M87 [2] have ushered us into a new era of black hole physics. Black hole thermodynamics has been a hot topic for research in black hole physics since the pioneering work [3–5], where Hawking and Bekenstein found that black holes can possess temperature and entropy. Analogous to the laws of thermodynamics, the four laws of black hole mechanics were established in [6].

Asymptotically AdS black holes can be in thermal equilibrium with the thermal radiation since the AdS boundary serves as a reflecting wall for the thermal radiation. Therefore, it is proper to study black hole thermodynamics for AdS black holes. Indeed, thermodynamic properties of AdS black holes were first investigated in [7], where the Hawking-Page phase transition between Schwarzschild AdS black holes and the thermal AdS space was discovered. With the advent of the AdS/CFT correspondence [8–10], there has been much interest in studying thermodynamics and phase structure of AdS black holes [11–19]. In particular, RNAdS black holes were observed to possess a van der Waals-like phase transition (i.e., a phase transition consisting of a first-order phase transition terminating at a second-order critical point) in a canonical ensemble [13,14] and a Hawking-Page-like phase transition in a grand canonical ensemble [20]. Alternatively, asymptotically flat black holes can be thermally stable with a dilaton potential [21,22], or by placing them inside a spherical cavity, on the wall of which the metric is fixed [23]. Early studies often concluded that black holes in a cavity have quite similar phase structure and transitions to the AdS counterparts [24–27]. However, it has recently been found that black holes in a cavity and the AdS counterparts can show different thermodynamic behavior, e.g., phase structure of Born-Infeld black holes [28,29], thermodynamic geometry of RN black holes [30] and the second law of thermodynamics [31].

However, unlike everyday thermodynamics, there is no pressure or volume associated with a black hole in the aforementioned black hole thermodynamics. To address this issue, the cosmological constant can be treated as a thermodynamic variable and interpreted as a thermodynamic pressure, which leads to the thermodynamics of black holes in the extended phase space [32–34]. The mass of black holes is then identified as the chemical enthalpy rather than the internal energy due to a pressure-volume term $V\delta P$ in the first law of thermodynamics [35]. The thermodynamic behavior has been investigated for various AdS black holes in the extended phase space [36–51], which discovered a broad range of new phenomena. For a recent review, see Ref. [34]. Especially for a RNAdS black hole, the coexistence line of the Hawking-Page phase transition in the P-T diagram is semi-infinite and reminiscent of the solid/liquid phase transition in a grand canonical ensemble [52], while the coexistence line in the P-T diagram is finite and terminates at a critical point in a canonical ensemble [33]. Intriguingly, more novel phase behavior has been found for more complicated black hole spacetimes. For example, reentrant phase transitions, which are composed of zeroth-order and first-order phase transitions, were discovered in Born-Infeld-AdS black holes [37,49], higher dimensional singly spinning Kerr-AdS black holes [53], AdS black holes in Lovelock

[*]guangzhouguo@stu.scu.edu.cn
[†]pengw@scu.edu.cn
[‡]iverwu@scu.edu.cn
[§]hyanga@scu.edu.cn

gravity [40], AdS black holes in dRGT massive gravity [54], and hairy AdS black holes [55]. A reentrant phase transition depicts a phenomenon that a system undergoes at least two phase transitions and returns to the macroscopically similar initial state under the monotonic variation of a thermodynamic variable. This phenomenon was first observed in a nicotine/water mixture, where a homogeneous mixture state transforms to a distinct nicotine/water phase as the temperature increases, and eventually return to the mixture state at a sufficiently high temperature [56]. Moreover, since the primary motivation to study AdS black holes is the AdS/CFT correspondence, there have been some interesting works understanding the extended phase space thermodynamics in the framework of the AdS/CFT correspondence [57–59]. It is noteworthy that the thermodynamics and phase structure of black holes in a cavity have been investigated in the extended phase space [60,61].

The no-hair theorem states that a black hole can be uniquely determined via its mass, electric charge and angular momentum [62–64]. Although this theorem can be proven when subjected to some specific energy conditions, e.g., the Einstein-Maxwell theory, various hairy black holes have been constructed to provide counterexamples to the no-hair theorem [65–71]. For a review, see Ref. [72]. Since testing the no-hair theorem is crucial to understand black hole physics, it is of great interest to find hairy black hole solutions and study their properties. To understand the formation of hairy black holes, authors of [73] proposed an Einstein-Maxwell-scalar (EMS) model with a nonminimal coupling between the scalar and electromagnetic fields, and studied the phenomenon of spontaneous scalarization in the model. Subsequently, various properties of this model and its extensions were discussed in the literature, e.g., different nonminimal coupling functions [74,75], dyons including magnetic charges [76], axionic-type couplings [77], massive and self-interacting scalar fields [78,79], horizonless reflecting stars [80], stability analysis of hairy black holes [81–85], higher dimensional scalar-tensor models [86], quasinormal modes of hairy black holes [87,88], two U(1) fields [89], quasitopological electromagnetism [90], topology and spacetime structure influences [91], the Einstein-Born-Infeld-scalar theory [92], with a negative cosmological constant [93], and images of hairy black holes with accretion flows [94,95]. In our recent work [96], we obtained asymptotically AdS hairy black hole solutions in the EMS model and investigated the phase structure of a canonical ensemble of RNAdS and hairy black holes in a normal phase space, where the cosmological constant is fixed. It showed that hairy and RNAdS black holes coexist in some parameter region, leading to a reentrant phase transition.

In this paper, focusing on the extended phase space, we discuss thermodynamic properties and phase structure of asymptotically AdS black hole solutions in the EMS model, which were obtained in [96]. Of particular interest is the observation that the EMS model exhibits a reentrant phase transition, which is composed of zeroth-order and second-order phase transitions between RNAdS and hairy black holes, in a certain parameter region. The remainder of this paper is organized as follows. In Sec. II, after we briefly review asymptotically AdS hairy black hole solutions in the EMS model, the Smarr relation, the first law of thermodynamics and the free energy are derived. In Sec. III, we study phase structure and transitions of hairy and RNAdS black holes in canonical and grand canonical ensembles by minimizing the free energy. We finally conclude our results in Sec. IV. We take $G = 1$ for simplicity throughout this paper.

II. THERMODYNAMICS

In this section, we first briefly review asymptotically AdS hairy black hole solutions in the EMS model. After the first law of thermodynamics is obtained by a covariant approach, we derive the Smarr relation using dimensional analysis and the Komar integral with respect to a timelike Killing vector. Finally, the free energy is computed in canonical and grand canonical ensembles, respectively, to study the phase structure and transitions of the hairy black holes.

A. Hairy black hole solutions

We consider an EMS model with a scalar field minimally coupled to the metric field and nonminimally coupled to the electromagnetic field, which is described by the action,

$$S_{\text{bulk}} = -\frac{1}{16\pi}\int d^4x\sqrt{-g}[R - 2\Lambda - 2(\partial\phi)^2 - f(\phi)F_{\mu\nu}F^{\mu\nu}]. \tag{1}$$

Here, $f(\phi)$ is a nonminimal coupling function between the scalar field ϕ and the electromagnetic field A_μ, $F_{\mu\nu} = \partial_\mu A_\nu - \partial_\nu A_\mu$ is the electromagnetic field strength tensor, and $\Lambda = -3/L^2$ is the cosmological constant with the AdS radius L. As in [96], we focus on the coupling function $f(\phi) = e^{\alpha\phi^2}$ with $\alpha \geq 0$ and the spherically symmetric ansatz for the metric, the electromagnetic field and the scalar field,

$$ds^2 = -N(r)e^{-2\delta(r)}dt^2 + \frac{1}{N(r)}dr^2 + r^2(d\theta^2 + \sin^2\theta d\varphi^2),$$
$$A_\mu dx^\mu = V(r)dt \quad \text{and} \quad \phi = \phi(r). \tag{2}$$

The equations of motion are

$$N'(r) = \frac{1-N(r)}{r} - \frac{Q^2}{r^3 e^{\alpha\phi^2(r)}} - rN(r)\phi'^2(r) + \frac{3r}{L^2},$$
$$(r^2N(r)\phi'(r))' = -\frac{\alpha\phi(r)Q^2}{e^{\alpha\phi^2(r)}r^2} - r^3N(r)\phi'^3(r),$$
$$\delta'(r) = -r\phi'^2(r),$$
$$V'(r) = \frac{Q}{r^2 e^{\alpha\phi^2(r)}}e^{-\delta(r)}, \tag{3}$$

where primes denote the derivatives with respect to the radial coordinate r, and the integration constant Q is interpreted as the electric charge of the black hole solution. For later use, we introduce the Misner-Sharp mass function $m(r)$ by $N(r) = 1 - 2m(r)/r + r^2/L^2$.

To solve the set of nonlinear ordinary differential equations (3), we impose appropriate boundary conditions at the event horizon of radius r_+ and the spatial infinity as

$$m(r_+) = \frac{r_+}{2} + \frac{r_+^3}{2L^2}, \quad \delta(r_+) = \delta_0, \quad \phi(r_+) = \phi_0, \quad V(r_+) = 0,$$
$$m(\infty) = M, \quad \delta(\infty) = 0, \quad \phi(\infty) = 0, \quad V(\infty) = \Phi, \tag{4}$$

where δ_0 and ϕ_0 are two positive constants, M is the ADM mass, and Φ is the electrostatic potential. It is worth noting that the electrostatic potential Φ is defined as

$$\Phi = A_t(\infty) - A_t(r_+) = V(\infty) - V(r_+), \tag{5}$$

which shows that a constant shift in $V(r)$ has no effect on Φ. Moreover, since the equations of motion (3) only involve $V'(r)$, the solution $V(r)$ can differ by an arbitrary constant. Therefore, one is free to choose a point where $V(r)$ is zero. Usually, it is practical to choose $V(r)$ at infinity to be zero, which leads to $\Phi = -A_t(r_+)$. Instead, in this paper, we shift the electrostatic potential $V(r)$ such that it vanishes at the horizon. Indeed, the condition $V(r_+) = 0$ is often adopted in holographic superconductor models [97–99].[1] Note that the general asymptotic scalar field solution is $\phi(r) \sim \phi_- + \frac{\phi_+}{r^3}$, where ϕ_+ can be interpreted as the expectation value of the dual operator of the scalar field on the conformal boundary in the presence of the external source ϕ_-. In this paper, we assume the absence of the external source, i.e., $\phi_- = 0$, which has been used in holographic applications with spontaneous symmetry breaking, e.g., holographic superconductors [100] and holographic superfluids [101]. Usually, the shooting method is used to obtain hairy black hole solutions of the nonlinear differential equations (3), which satisfy the boundary conditions (4). Here, we use the NDSolve function in Wolfram *Mathematica* to numerically solve the differential equations (3).

The hairy black hole solutions can be characterized by the number n of nodes of the scalar field. In [96], it was demonstrated that the fundamental branch of the solutions, i.e., $n = 0$, is stable against radial perturbations, whereas the $n = 1$ and 2 excited branches are not. Therefore, we focus on the fundamental branch in this paper. Note that RNAdS black holes with the scalar field $\phi = 0$ also are solutions of the EMS model (1). In fact, RNAdS and hairy black hole solutions coexist in a certain parameter region [96]. As shown in Fig. 1, the domain of existence of RNAdS black holes is presented below the horizon dashed line, which represents extremal RNAdS black holes. On the bifurcation line (the blue dashed line), there appears a zero mode of the scalar field perturbation, which leads to black hole solutions with a scalar hair [96]. The coexistence region of RNAdS and hairy black holes is bounded by the bifurcation and extremal RNAdS black hole lines. Although we mainly focus on hairy black holes with a nontrivial profile for the scalar field ϕ in this paper, our results below also apply to RNAdS black holes in the limit of $\phi = 0$.

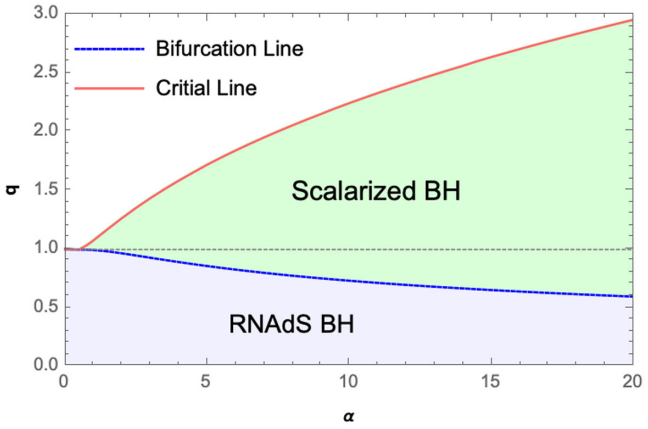

FIG. 1. Domains of existence of hairy and RNAdS black holes in the α-q plane for $Q/L = 0.1$. Hairy black holes exist in the light green region, which is bounded by the bifurcation line (the dashed blue line) and the critical line (the red line). On the other hand, RNAdS black holes appear below the horizontal dashed gray line, on which RNAdS black holes are extremal. There exists an overlapping region of hairy and RNAdS black holes between the bifurcation and extremal RNAdS black hole lines, where hairy and RNAdS black holes can coexist.

[1]Consider a holographic superconductor model with a complex scalar field Ψ of charge q and mass m in a black hole spacetime of the metric

$$ds^2 = g_{tt}(r)dt^2 + g_{rr}(r)dr^2 + r^2(d\theta^2 + \sin^2\theta d\varphi^2),$$

where an event horizon is at $r = r_+$. Moreover, one can use gauge invariance to conveniently make the scalar field Ψ real. Assuming the electromagnetic field $A_\mu dx^\mu = V(r)dt$ and $\Psi = \psi(r)$, the scalar field Lagrangian becomes

$$-|(\partial_\mu - iqA_\mu)\Psi|^2 - m^2|\Psi|^2 \to -g^{rr}(r)[\partial_r\psi(r)]^2 - m_{\text{eff}}^2\psi^2(r),$$

where the effective mass of the scalar field is

$$m_{\text{eff}}^2 = m^2 + q^2 g^{tt}(r)V^2(r).$$

Since $g^{tt}(r) \to -\infty$ as $r \to r_+$ outside the black hole horizon, m_{eff}^2 is always below the Breitenlohner–Freedman bound just outside the horizon if $V(r_+)$ is nonzero, which means that the scalar field is unstable at the horizon, rendering the black hole background unstable under scalar perturbations. In addition, the electric current $\psi^2(r)A_\mu$ must remain finite at the horizon, which requires that $g^{\mu\nu}A_\mu A_\nu$ remains finite at the horizon, leading to $V(r_+) = 0$.

B. First law of thermodynamics and thermodynamic volume

In the extended phase space, we use the Iyer and Wald's covariant construction [102–106] to obtain the first law of thermodynamics for hairy black holes. We start with a 4-form Lagrangian $\mathbf{L}$, which is diffeomorphism invariant and satisfies

$$\mathbf{L}(f^*\psi) = f^*(\mathbf{L}(\psi)). \tag{6}$$

Here, ψ collectively denotes various fields, including the metric $g_{\mu\nu}$, the electromagnetic field A_μ and other dynamical fields, f^* represents the pullback after a diffeomorphism map f, and $*$ is the Hodge star operator. Alternatively, an equivalent description of diffeomorphism invariant (6) is

$$\delta_\xi \mathbf{L} = \mathcal{L}_\xi \mathbf{L} = *E\mathcal{L}_\xi\psi + d(*\theta), \tag{7}$$

which relates the variation alone a vector field ξ to a corresponding Lie derivative $\mathcal{L}_\xi$. Here, E schematically denotes the equations of motion with respect to ψ, and the symplectic potential form θ is an one-form. Subsequently, we define a current

$$*j_\xi = *\theta(\psi, \mathcal{L}_\xi\psi) - \xi\cdot\mathbf{L}. \tag{8}$$

By virtue of Eq. (7), an exterior derivative acting on the current (8) then yields

$$d(*j_\xi) = -*E\mathcal{L}_\xi\psi, \tag{9}$$

which shows that the current is conserved if the equations of motion are satisfied. In particular, this current is thus referred to as the Noether current associated with the diffeomorphism symmetry. Consequently, there is a 2-form Noether charge $*Q_\xi$ related to the vector field ξ, which is constructed by

$$*j_\xi = d(*Q_\xi). \tag{10}$$

In general, a symplectic form $\omega(\psi, \delta_1\psi, \delta_2\psi)$ can be built up with an one-form $\theta(\psi, \delta\psi)$,

$$\omega(\psi, \delta_1\psi, \delta_2\psi) \equiv \delta_2(*\theta(\psi, \delta_1\psi)) - \delta_1(*\theta(\psi, \delta_2\psi)). \tag{11}$$

Replacing one of variations with the Lie derivative, i.e., $\delta \to \mathcal{L}_\xi$, gives the special symplectic form $\omega(\psi, \delta\psi, \mathcal{L}_\xi\psi)$,

$$\omega(\psi, \delta\psi, \mathcal{L}_\xi\psi) = d(\delta(*Q) - i_\xi(*\theta(\psi, \delta\psi))) + i_\xi(*E\delta\psi). \tag{12}$$

Furthermore, integrating this special symplectic form over a Cauchy surface Σ leads to the variation of Hamiltonian [104,106],

$$\begin{aligned}\delta H_\xi &= \int_\Sigma \omega(\psi, \delta\psi, \mathcal{L}_\xi\psi) \\ &= \int_{\partial\Sigma} (\delta(*Q_\xi) - \xi\cdot(*\theta)) + \int_\Sigma \xi\cdot(*E\delta\psi).\end{aligned} \tag{13}$$

In practice, the Cauchy surface Σ is generally chosen as a constant time hypersurface, whose boundary $\partial\Sigma$ is composed of the 2-spheres at the event horizon and the spatial infinity. The variation of Hamiltonian δH_ξ should vanish if ξ is a Killing vector, i.e., $\mathcal{L}_\xi\psi = 0$. Note that if some background variables, e.g., the cosmological constant, are treated as dynamical fields, the associated equations of motion are not necessarily satisfied, and hence the last term in Eq. (13) can make nonvanishing contributions [105,106].

To derive the first law of thermodynamics for hairy black holes, we apply the identity (13) to hairy black hole solutions with a timelike Killing vector $\xi = \partial_t$. We first derive the explicit expression of Eq. (7) by varying the action (1),

$$\delta S_{\rm bulk} = \int d^4x\sqrt{-g}(E^g_{\mu\nu}\delta g^{\mu\nu} + E^A_\mu\delta A^\mu + E^\phi\delta\phi + \nabla_\mu\theta^\mu), \tag{14}$$

where

$$\begin{aligned}E^g_{\mu\nu} &= -\frac{1}{16\pi}\Big\{R_{\mu\nu} - \frac{1}{2}Rg_{\mu\nu} + \Lambda g_{\mu\nu} \\ &\quad - 2\Big[\nabla_\mu\phi\nabla_\nu\phi - \frac{1}{2}g_{\mu\nu}(\partial\phi)^2 \\ &\quad + e^{\alpha\phi^2}\Big(F_{\mu\rho}F_\nu{}^\rho - \frac{1}{4}g_{\mu\nu}F^2\Big)\Big]\Big\}, \\ E^A_\mu &= -\frac{1}{4\pi}\nabla^\rho(e^{\alpha\phi^2}F_{\rho\mu}), \\ E^\phi &= -\frac{1}{4\pi}\Big(\nabla^2\phi - \frac{1}{2}\alpha\phi e^{\alpha\phi^2}F^2\Big),\end{aligned} \tag{15}$$

and the symplectic potential form θ^μ is

$$\begin{aligned}\theta^\mu = -\frac{1}{16\pi}&[\nabla^\mu(g_{\rho\sigma}\delta g^{\rho\sigma}) - \nabla_\nu(\delta g^{\mu\nu}) \\ &- 4g^{\mu\nu}\nabla_\nu\phi\delta\phi - 4f(\phi)F^{\mu\nu}\delta A_\nu].\end{aligned} \tag{16}$$

The current $*j_\xi$ can be obtained by using Eq. (8),

$$\begin{aligned}*j_\xi = \frac{1}{3!}\epsilon_{\mu\nu\rho\sigma}&\Big[\theta^\mu + \frac{1}{16\pi}(R - 2\Lambda - 2(\partial\phi)^2 - e^{\alpha\phi^2}F^2)\xi^\mu\Big] \\ &\times dx^\nu\wedge dx^\rho\wedge dx^\sigma.\end{aligned} \tag{17}$$

To construct the Noether charge $*Q_\xi$, one can supply the formula (10) with a combination of Eq. (15), which does not contribute under the on-shell condition. Specifically, the exterior derivative acting on the Noether charge is

$$d(*Q_\xi) = *[j_\xi - \xi^\beta(2E^g_{\mu\beta} - E^A_\mu A_\beta)dx^\mu] = -\frac{1}{3!}\epsilon_{\mu\nu\rho\sigma}\nabla_\beta Q^{\beta\mu}_\xi dx^\nu \wedge dx^\rho \wedge dx^\sigma, \quad (18)$$

with

$$Q^{\beta\mu}_\xi = \frac{1}{16\pi}(\nabla^\beta\xi^\mu - \nabla^\mu\xi^\beta + 4e^{\alpha\phi^2}F^{\beta\mu}A_\alpha\xi^\alpha). \quad (19)$$

Subsequently, substituting Eq. (19) into the first term of the right-hand side of Eq. (13) yields

$$\int_{\partial\Sigma}\delta(*Q_\xi) = -\frac{1}{16\pi}\delta\int_{\partial\Sigma}d\theta d\phi r^2\sin\theta n^t\sigma^r \times\left[\nabla_t\xi_r - \nabla_r\xi_t - 4\frac{Q}{r^2}e^{-\delta(r)}A_t(r)\right], \quad (20)$$

where $n^\mu = (N^{-1/2}(r)e^{\delta(r)},0,0,0)$ and $\sigma^\mu = (0,N^{1/2}(r),0,0)$. Furthermore, we apply the asymptotic behaviors (4) to Eq. (20) to obtain

$$\int_{r=+\infty}\delta(*Q_\xi) = \Phi\delta Q, \qquad \int_{r=r_+}\delta(*Q_\xi) = -T\delta S, \quad (21)$$

where $T \equiv e^{-\delta(r_+)}N'(r_+)/4\pi$ is the Hawking temperature, and $S \equiv \pi r_+^2$ is the black hole entropy. In the second line of Eq. (21), we use the relation for surface gravity $\kappa_+\epsilon^{\mu\nu} = \nabla^\mu\xi^\nu$, which is associated with the Hawking temperature via $T = \kappa_+/2\pi$ [105]. In analogy, with the help of Eqs. (4) and (16), one has

$$-\int_{\partial\Sigma}\xi\cdot(*\theta) = \left(\frac{1}{2}re^{-\delta(r)}\delta N + r^2e^{-\delta(r)}N(r)\phi'(r)\delta\phi\right)\Big|_{r=+\infty} = -\delta M - \frac{\delta\Lambda e^{-\delta(r)}r^3}{6}\Big|_{r=+\infty}, \quad (22)$$

where $\xi = 0$ at the event horizon is used. Moreover, we allow the cosmological constant to be varied as a dynamical field, which gives contributions to Eq. (13) with

$$\int_\Sigma\xi\cdot(*E\delta\phi) = \frac{1}{2}\int_{r_+}^{+\infty}drr^2e^{-\delta(r)}\delta\Lambda = \frac{\delta\Lambda e^{-\delta(r)}r^3}{6}\Big|_{r=r_+}^{r=+\infty} + \int_{r_+}^{\infty}dr\delta'(r)e^{-\delta(r)}\frac{\delta\Lambda r^3}{6}. \quad (23)$$

Since $\delta H_\xi = 0$ for the Killing vector $\xi = \partial_t$, one arrives at the first law of thermodynamics for hairy black holes in the extended phase space,

$$\delta M = T\delta S + \Phi\delta Q + \left(e^{-\delta_0}\frac{4\pi r_+^3}{3} - \int_{r_+}^{\infty}dr\delta'(r)e^{-\delta(r)}\frac{4\pi r^3}{3}\right)\delta P, \quad (24)$$

where $P \equiv -\Lambda/8\pi = 3/8\pi L^2$ is the thermodynamic pressure. Note that the mass M plays the role of an enthalpy in the extended phase space. Accordingly, the conjugate thermodynamic volume is given by

$$V = \left(\frac{\partial M}{\partial P}\right)_{S,Q} = e^{-\delta_0}\frac{4\pi r_+^3}{3} - \int_{r_+}^{\infty}dr\delta'(r)e^{-\delta(r)}\frac{4\pi r^3}{3}. \quad (25)$$

For a RNAdS black hole with $\delta(r) = 0$, the thermodynamic volume reduces to $V = 4\pi r_+^3/3$.

In Fig. 2, we display the thermodynamic volume as a function of $q \equiv Q/M$ for RNAdS black holes and hairy black holes with $\alpha = 5$, 10 and 15. It shows that hairy hole solutions bifurcate from RNAdS black hole solutions. In the coexisting region, for a given q, the hairy black holes have a larger thermodynamic volume than the RNAdS black hole. Moreover, the thermodynamic volume of hairy black holes becomes larger for a stronger α. We also calculate the isoperimetric ratio,

$$R \equiv \left(\frac{3V}{4\pi r_+^3}\right)^{\frac{1}{3}}, \quad (26)$$

for the RNAdS and hairy black holes, which is represented by the color of lines in Fig. 2. In fact, it was conjectured in [107] that a reverse isoperimetric inequality $R \geq 1$ holds for AdS black holes. Interestingly, several black hole solutions

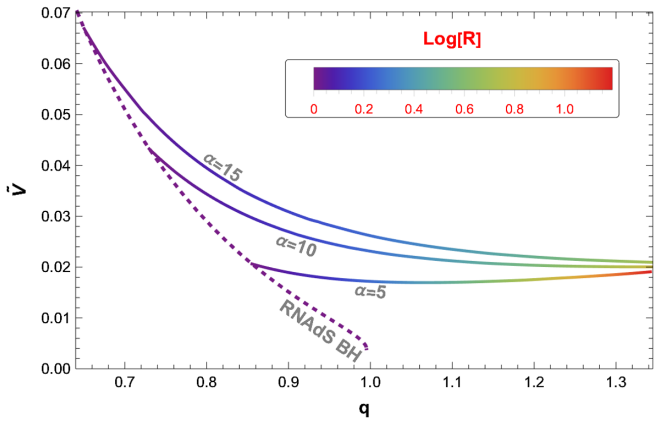

FIG. 2. Reduced thermodynamic volume $\tilde{V} \equiv V/L^3$ versus $q \equiv Q/M$ for RNAdS black holes and hairy black holes with $\alpha = 5$, 10 and 15. The color of lines specifies the value of $\log R$, where R is the isoperimetric ratio. The hairy black holes have a larger thermodynamic volume than the RNAdS black hole of the same q, and satisfy the reverse isoperimetric inequality $R \geq 1$.

have been found to violate the reverse isoperimetric inequality [108–111]. Figure 2 shows that the RNAdS and hairy black holes satisfy the reverse isoperimetric inequality, i.e., $\log R \geq 0$.

C. Smarr relation

The Smarr relation, which relates various quantities of black holes, plays an important role in black hole thermodynamics [112]. Using the Euler's formula for homogeneous functions, the Smarr relation can be derived from the first law of thermodynamics (24), which relates various differential quantities. In fact, due to the Euler's theorem, we can write the black hole mass $M = M(S, P, Q)$ as

$$\begin{aligned} M &= 2\frac{\partial M}{\partial S}S - 2\frac{\partial M}{\partial P}P + \frac{\partial M}{\partial Q}Q \\ &= 2TS - 2PV + \Phi Q, \end{aligned} \tag{27}$$

where we use $[M] = [Q] = [L]$, $[S] = [L]^2$ and $[P] = [L]^{-2}$, and the partial derivatives can be expressed in terms of black hole quantities via the first law of thermodynamics. Note that there is no contribution from the coupling parameter α to the Smarr relation since α is dimensionless.

Alternatively, the Smarr relation can also be derived by geometric means [6,35]. To obtain the Smarr relation, we consider a hypersurface Σ with the boundary $\partial\Sigma$ in a manifold $\mathcal{M}$ endowed with a timelike Killing vector $\xi = \partial_t$. Due to Gauss's law and Einstein's equations, an identity for a Killing vector $\nabla_\mu\nabla_\nu\xi^\mu = \xi^\mu R_{\mu\nu}$ can be integrated on Σ,

$$\int_{\partial\Sigma} dS_{\mu\nu}\nabla^\mu\xi^\nu = \int_\Sigma dS^\mu\xi^\nu\left(2T_{\mu\nu} - Tg_{\mu\nu} - \frac{3g_{\mu\nu}}{L^2}\right), \tag{28}$$

where $dS_{\mu\nu}$ is the surface element normal to $\partial\Sigma$, dS_μ is correspondingly the volume element on Σ, and $T_{\mu\nu}$ is the energy-momentum tensor. For the hairy black hole, we choose the hypersurface of constant time t bounded by the event horizon and the spatial infinity, such that the boundary $\partial\Sigma$ consists of the 2-spheres at $r = r_+$ and $r = \infty$. The left-hand side of Eq. (28) becomes

$$\begin{aligned} \int_{\partial\Sigma} dS_{\mu\nu}\nabla^\mu\xi^\nu &= \int_{\partial\Sigma} d^2x\sqrt{\gamma^{(2)}}n_\mu\sigma_\nu(\nabla^\mu\xi^\nu) \\ &= 4\pi r^2\frac{e^{-\delta(r)}}{2}[N'(r) - 2N(r)\delta'(r)]\Big|_{r=r_+}^{r=+\infty}, \end{aligned} \tag{29}$$

where $\sigma_\mu = (0, N^{1/2}(r), 0, 0)$, $n_\mu = (N^{-1/2}(r)e^{\delta(r)}, 0, 0, 0)$, $\xi^\mu = (1, 0, 0, 0)$, and $\gamma^{(2)}$ is the induced metric of the 2-spheres at $r = r_+$ and $r = \infty$. Using the equations of motion (3) and

$$\begin{aligned} T_{\mu\nu} &= \partial_\mu\phi\partial_\nu\phi - \frac{1}{2}g_{\mu\nu}(\partial\phi)^2 \\ &\quad + e^{\alpha\phi^2}\left(F_{\mu\rho}F_\nu{}^\rho - \frac{1}{4}g_{\mu\nu}F_{\rho\sigma}F^{\rho\sigma}\right), \end{aligned} \tag{30}$$

one can express the right-hand side of Eq. (28) as

$$\begin{aligned} &\int_\Sigma dS^\mu\xi^\nu\left(2T_{\mu\nu} - Tg_{\mu\nu} - \frac{3g_{\mu\nu}}{L^2}\right) \\ &= \int_\Sigma drd\theta d\phi r^2\sin\theta n^\mu\xi^\nu\left(2T_{\mu\nu} - Tg_{\mu\nu} - \frac{3g_{\mu\nu}}{L^2}\right) \\ &= 4\pi\int_{r_+}^\infty dre^{-\delta(r)}\left(\frac{Q^2}{r^2e^{\alpha\phi^2(r)}} + \frac{3}{L^2}r^2\right) \\ &= 4\pi\left\{\left[e^{-\delta(r)}\frac{r^3}{L^2} + QV'(r)\right]\Big|_{r=r_+}^{r=+\infty}\right. \\ &\quad \left. + \int_{r_+}^\infty dre^{-\delta(r)}\delta'(r)\frac{r^3}{L^2}\right\}. \end{aligned} \tag{31}$$

Then the identity (28) reduces to

$$M - 2TS = Q\Phi - e^{-\delta_0}\frac{r_+^3}{L^2} + \int_{r_+}^\infty dre^{-\delta(r)}\delta'(r)\frac{r^3}{L^2}, \tag{32}$$

where we use the boundary conditions (4) for $N(r)$, $\delta(r)$, and $V(r)$ at $r = r_+$ and $r = +\infty$. With the help of $P = 3/8\pi L^2$ and Eq. (25), the above equation becomes the Smarr relation (27).

D. Free energy

The free energy plays a crucial role in studying phase structure and transitions of black holes. The free energy of a black hole can be obtained by computing the associated Euclidean path integral, which is related to a thermal partition function. Specifically, the thermal partition function is usually computed in the semiclassical approximation by exponentiating the on-shell Euclidean action $S^E_{\text{on-shell}}$,

$$Z \sim e^{-S^E_{\text{on-shell}}}, \tag{33}$$

where $S^E_{\text{on-shell}}$ is the on-shell Euclidean action.

For the hairy black hole solutions, $S^E_{\text{on-shell}}$ usually diverges on the AdS boundary, which requires some boundary treatments to regularize the bulk action (1). For example, one can regularize the on-shell Euclidean action of AdS black holes by placing them in a spherical cavity with a finite radius, which serves as a cutoff for the AdS boundary [20]. Alternatively, the on-shell Euclidean action can be regularized by adding some counterterms to remove the divergent contribution from the AdS boundary. The regularized action S_R is given by [113–118]

$$S_R = S_{\text{bulk}} + S_{\text{GH}} + S_{\text{ct}}, \tag{34}$$

where the Gibbon-Hawking boundary term S_{GH} is introduced to render the variational principle well-posed, and the counterterm S_{ct} is constructed to cancel divergences on asymptotic boundaries. Specifically, these two boundary terms are evaluated on the hypersurface at the spatial infinity with the induced metric γ,

$$S_{\text{GH}} = -\frac{1}{8\pi}\int d^3x\sqrt{-\gamma}\Theta,$$
$$S_{\text{ct}} = \frac{1}{8\pi}\int d^3x\sqrt{-\gamma}\left(\frac{2}{L}+\frac{L}{2}R_3\right), \tag{35}$$

where Θ is the trace of the extrinsic curvature $\Theta_{\mu\nu}$, and R_3 is the scalar curvature of the induced metric γ. To derive the extrinsic curvature $\Theta_{\mu\nu}$, we first introduce a projection operator

$$h_{\mu\nu} \equiv g_{\mu\nu} - \sigma_\mu\sigma_\nu, \tag{36}$$

with $\sigma_\mu = (0, N^{-1/2}(r), 0, 0)$. Therefore, the extrinsic curvature is defined by

$$\Theta_{\mu\nu} = -\frac{1}{2}h^\rho_\mu h^\sigma_\nu(\nabla_\rho\sigma_\sigma + \nabla_\sigma\sigma_\rho), \tag{37}$$

which yields

$$\Theta = \frac{1}{2}N^{-1/2}(r)N'(r) - \delta'(r)N^{1/2}(r) + 2\frac{N^{1/2}(r)}{r}. \tag{38}$$

Using the equations of motion (3) and the boundary conditions (4), we obtain

$$S^E_{\text{bulk,on-shell}} = \frac{1}{T}\left(\frac{e^{-\delta(r)}r^2N'(r) - 2e^{-\delta(r)}r^2N(r)\delta'(r)}{4}\bigg|_{r=+\infty} - TS - Q\Phi\right),$$
$$S^E_{\text{GH,on-shell}} = -\frac{1}{T}\left[\frac{e^{-\delta(r)}r^2N'(r) - 2e^{-\delta(r)}r^2\delta'(r)N(r)}{4} + e^{-\delta(r)}\left(r - 2M + \frac{r^3}{L^2}\right)\right]\bigg|_{r=+\infty},$$
$$S^E_{\text{ct,on-shell}} = \frac{e^{-\delta(r)}}{T}\left(\frac{r^3}{L^2} + r - M\right)\bigg|_{r=+\infty}. \tag{39}$$

The free energy of hairy black hole solutions is then given by

$$F = TS^E_{\text{R,on-shell}} = M - TS - Q\Phi. \tag{40}$$

It is deserved to mention that the variational problem is well defined only when the potential Φ is fixed on the boundaries, which means that the free energy (40) is properly used in a grand canonical ensemble at a constant potential. On the other hand, the electric charge Q is fixed in a canonical ensemble. To construct an appropriate free energy in a canonical ensemble, the regularized action should be supplied with an additional boundary term [49],

$$S_{\text{surf}} = -\frac{1}{4}\int d^3x\sqrt{\gamma}f(\phi)F^{\mu\nu}n_\mu A_\nu. \tag{41}$$

This surface term gives an extra contribution to the on-shell Euclidean action, $S^E_{\text{surf,on-shell}} = \frac{Q\Phi}{T}$, which leads to the free energy in a canonical ensemble,

$$F = M - TS. \tag{42}$$

III. PHASE STRUCTURE AND TRANSITIONS

In this section, we investigate phase structure and transitions of RNAdS and hairy black holes in a grand canonical ensemble and a canonical ensemble. For later convenience, we define the following reduced quantities,

$$\tilde{T} = TL, \qquad \tilde{F} = F/L, \qquad \tilde{r}_+ = r_+/L,$$
$$\tilde{Q} = Q/L, \qquad \tilde{M} = M/L, \tag{43}$$

where the AdS radius $L = \sqrt{3/(8\pi P)}$. The accuracy of our numerical results is tested using the Smarr relation, which estimates the numerical error to be around 10^{-6}. Without loss of generality, we focus on $\alpha = 5$ in the remainder of this section.

A. Grand canonical ensemble

In a grand canonical ensemble, black holes are maintained at a constant temperature T and a constant potential Φ. To express thermodynamic quantities in terms of T and Φ, we first need to find the horizon radius r_+ as a function of T and Φ. If the function $r_+(T,\Phi)$ is multivalued, there is more than one black hole phase, corresponding to different branches of $r_+(T,\Phi)$.

The upper panels of Figs. 3 and 4 show the dependence of the reduced event horizon radius $\tilde{r}_+$ of RNAdS (blue lines) and hairy (green lines) black holes on their reduced temperature $\tilde{T}$ for several representative values of the potential Φ. When $\tilde{r}_+$ is a monotonic function of $\tilde{T}$, there is one branch (phase) for the black hole, e.g., the hairy

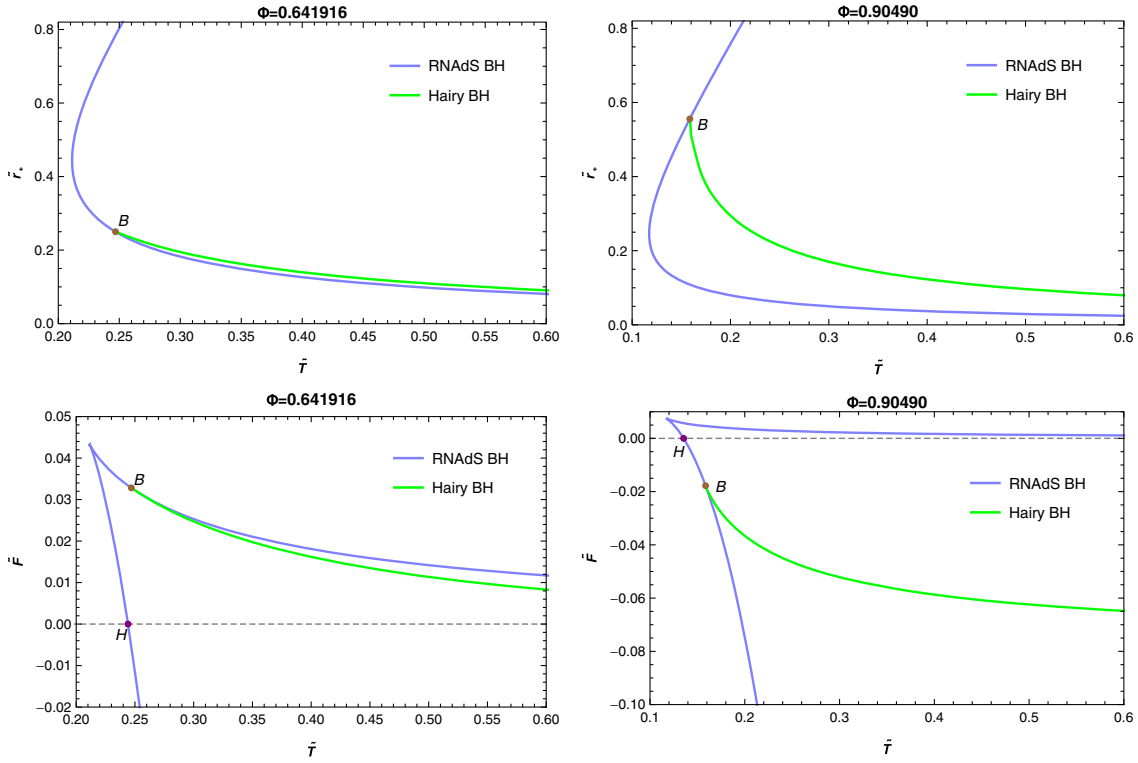

FIG. 3. Plots of the reduced horizon radius $\tilde{r}_+$ (upper row) and the reduced free energy $\tilde{F}$ (lower row) versus the reduced temperature $\tilde{T}$ for RNAdS (blue lines) and hairy (green lines) black holes with $\alpha = 5$ in the grand canonical ensemble. Dashed horizontal lines represent the thermal AdS space, and bifurcation points are labeled by B. We consider two cases with $\Phi = 0.641916$ (left column) and 0.90490 (right column), in which hairy black holes have only one phase. For RNAdS black holes, $\tilde{r}_+(\tilde{T})$ is double-valued, corresponding to the large RNAdS BH phase (the branch with a larger horizon radius) and the small RNAdS BH phase (the branch with a smaller horizon radius). A first-order phase transition between the thermal AdS space and large RNAdS BH occurs at the point H.

black holes in Fig. 3 and the RNAdS black hole in the upper-right panel of Fig. 4. When $\tilde{r}_+(\tilde{T})$ is double-valued in some range of $\tilde{T}$, there exist two branches of black hole solutions with different horizon radii for a given $\tilde{T}$, e.g., the RNAdS black holes in Fig. 3 and the upper-left panel of Fig. 4, and the hairy black holes in Fig. 4. Usually, the upper branch is dubbed as the large BH phase while the lower one is the small BH phase. To investigate phase transitions between different black holes phases, in the lower panels of Figs. 3 and 4, we plot the reduced free energy $\tilde{F}$ against the reduced temperature $\tilde{T}$ for RNAdS and hairy black holes with the same $\tilde{T}$ as that in the corresponding upper panels. Note that the extremum of the function $\tilde{T}(\tilde{r}_+)$ in the upper panels corresponds to the cusp of $\tilde{F}(\tilde{T})$ in the lower panels. Moreover, the bifurcation points B correspond to the bifurcation line in Fig. 1, where hairy black holes merge with RNAdS black holes. From the cusps of free energies and the bifurcation points, one can associate the branches of the free energies in the lower panels with the corresponding black hole phases in the upper panels. For instance, in the lower-left panel of Fig. 4, the lower blue branch of RNAdS black holes has the bifurcation point B, and hence is the free energy of the upper blue branch with B in the upper-left panel. In other words, the large RNAdS BH phase has a lower free energy than the smaller one. Since the neutral thermal AdS space with a fixed potential Φ is also the solution of the equations of motion (3), the thermal phases of the EMS model in a grand canonical ensemble consist not only of RNAdS and hairy black hole phases but also of the thermal AdS space, whose free energy is displayed as a dashed horizontal line in Figs. 3 and 4. The globally stable phase of the EMS model corresponds to the thermal phase of lowest free energy. As the temperature increases, a phase transition occurs whenever a phase, whose free energy initially is not the global minimum, becomes the new globally stable phase.

In the small Φ regime, Fig. 3 displays $\tilde{r}_+(\tilde{T})$ and $\tilde{F}(\tilde{T})$ for RNAdS and hairy black holes with $\Phi = 0.641916$ and 0.90490. As shown in the upper row, the RNAdS black hole solutions possess two branches of different horizon radii, dubbed large and small RNAdS BHs, respectively, whereas the hairy black hole solutions have only one branch. Moreover, the hairy black holes bifurcate from the RNAdS black holes at bifurcation points B, which determine the minimum temperature of the hairy black holes. The lower row shows that the hairy black hole phase cannot be the globally stable against large RNAdS BH (the branch

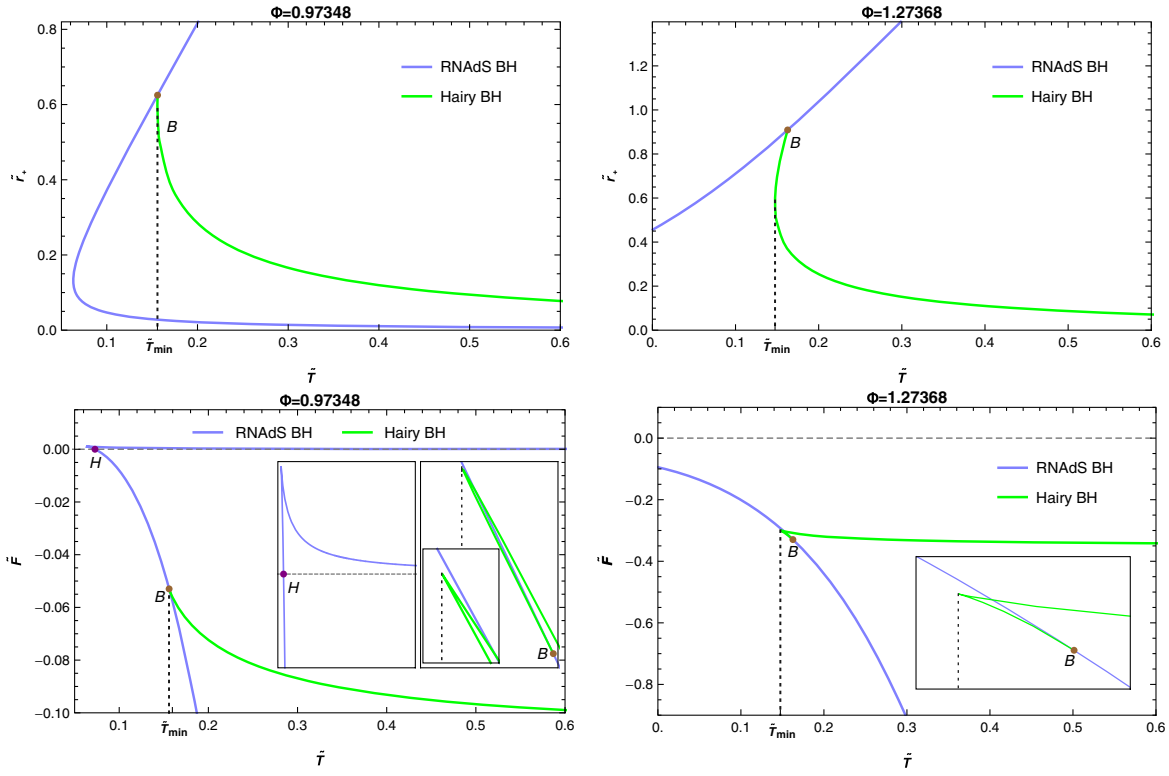

FIG. 4. Plots of the reduced horizon radius $\tilde{r}_+$ (upper row) and the reduced free energy $\tilde{F}$ (lower row) versus the reduced temperature $\tilde{T}$ for RNAdS (blue lines) and hairy (green lines) black holes with $\alpha = 5$ in the grand canonical ensemble. Dashed horizontal lines represent the thermal AdS space, and bifurcation points are labelled by B. When $\Phi = 0.97348$ and 1.27368, there are two phases of hairy black holes, large and small hairy BHs, which exist above the minimum temperature $\tilde{T}_{\min}$ (vertical dotted lines). Left column: $\Phi = 0.97348$. RNAdS black holes have two phases, large and small RNAdS BHs. Increasing the temperature from $\tilde{T} = 0$, the system follows the dashed line of the thermal AdS space until the point H, where a first-order phase transition to large RNAdS BH occurs. Further increasing $\tilde{T}$, the system jumps to the lower green line of large hairy BH, which corresponds to a zeroth-order phase to large hairy BH. As $\tilde{T}$ continues to increase, the system follows the lower green line until it joins the blue line at the bifurcation point B, which indicates a second-order phase transition to large RNAdS BH. In a nutshell, the system undergoes the Hawking-Page phase transition and a large RNAdS BH/large hairy BH/large RNAdS BH reentrant phase transition. Right column: $\Phi = 1.27368$. RNAdS black hole solutions have only one phase, dubbed RNAdS BH. As $\tilde{T}$ increases, a RNAdS BH/large hairy BH/RNAdS BH reentrant phase transition occurs, consisting of a zeroth-order phase transition at $\tilde{T}_{\min}$ and a second-order phase transition at the bifurcation point B.

with a larger horizon radius) since large RNAdS BH always has a lower free energy than the hairy black hole. For a temperature greater/less than that of the point H, large RNAdS BH/thermal AdS space is globally stable, which leads to the first-order Hawking-Page phase transition at the point H.

For a large enough value of Φ, hairy black holes can possess two phases, namely the large and small hairy BH phases. In Fig. 4, we present $\tilde{r}_+$ and $\tilde{F}$ as functions of $\tilde{T}$ for RNAdS and hairy black holes with $\Phi = 0.97348$ and 1.27368. It is observed that there are two phases for the hairy black holes in both cases, while the RNAdS black holes have one (two) phase(s) for $\Phi = 0.97348(1.27368)$. Moreover, the hairy black holes have a minimum temperature $\tilde{T}_{\min}$, and large hairy BH coexists with small hairy BH between $\tilde{T} = \tilde{T}_{\min}$ and the bifurcation points B, where large hairy BH and RNAdS black holes merge. When $\Phi = 0.97348$, RNAdS black hole solutions have two branches, corresponding to large and small RNAdS BHs. As $\tilde{T}$ increases from zero, there occurs a first-order phase transition from the thermal AdS space to large RNAdS BH at the purple point H. Subsequently, the left inset of the lower panel shows that the globally stable phase jumps to large hairy BH from large RNAdS BH, which signals a zeroth-order phase transition occurring at $\tilde{T} = \tilde{T}_{\min}$. Further increasing $\tilde{T}$, we observe that the globally stable phase remains large hairy BH until the bifurcation point B, where the system undergoes a second-order phase transition and returns to large RNAdS BH. Note that hairy and RNAdS black holes have the same entropy at the bifurcation point, thus indicating the phase transition at the bifurcation point is second-order. In short, a RNAdS BH/hairy BH/RNAdS BH reentrant phase transition is observed as $\tilde{T}$ increases. When $\Phi = 1.27368$, RNAdS black hole solutions have only one phase, whose free energy is always smaller than that of the thermal AdS

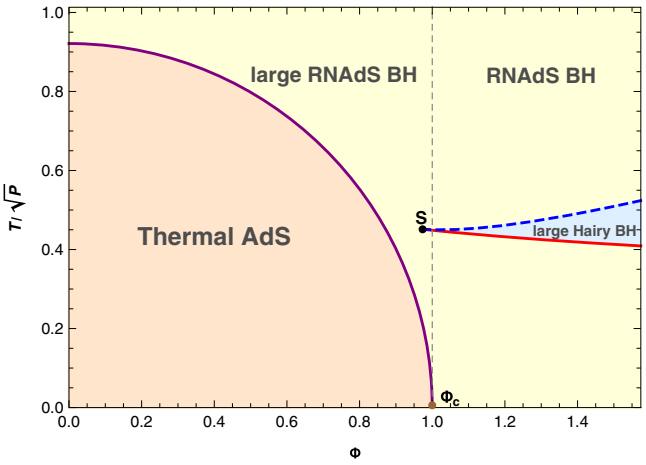

FIG. 5. Phase diagram of the grand canonical ensemble of hairy and RNAdS black holes with $\alpha = 5$ in the Φ-$T/\sqrt{P}$ plane. A first-order phase transition line (purple line) separates the thermal AdS space and large RNAdS BH, and terminates at $\Phi = \Phi_c$. In the large Φ regime, large hairy BH appears, and is bounded by a zeroth-order phase transition line (red line) and a second-order one (blue dashed line).

space. So there is no Hawking-Page first-order phase transition, However, as shown in the inset of the lower panel, a RNAdS BH/large hairy BH/RNAdS BH reentrant phase transition still occurs.

In addition, it is of interest to consider local thermal stability of black hole solutions against thermodynamic fluctuations. In a grand canonical ensemble, a specific heat at constant potential and pressure,

$$C_{\Phi,P} = T\left(\frac{\partial S}{\partial T}\right)_{\Phi,P} = \frac{3\tilde{r}_+\tilde{T}}{4P}\left(\frac{\partial \tilde{r}_+}{\partial \tilde{T}}\right)_{\Phi,P}, \tag{44}$$

can be used to analyze the thermal stability. Specially, the thermal stability of a black hole phase follows from $C_{\Phi,P} > 0$ (or equivalently, $\partial\tilde{r}_+/\partial\tilde{T} > 0$). From the upper rows of Figs. 3 and 4, we notice that the globally stable phases of RNAdS and hairy black holes possess a positive C_Q, and are thermally stable.

To better illustrate phase structure and transitions of hairy and RNAdS black holes, we plot phase diagrams in the Φ-$T/\sqrt{P}$ and P-T planes in Figs. 5 and 6, respectively, where $\alpha = 5$. These phase diagrams exhibit the globally stable phases, which possess the lowest free energy, and the phase transitions between them. In Figs. 5 and 6, purple lines correspond to first-order phase transitions between the thermal AdS space and large RNAdS BH, red lines to zeroth-order phase transitions between RNAdS black holes and large hairy BH, and blue dashed lines to second-order phase transitions between large hairy BH and RNAdS black holes.

In the phase diagram in the Φ-$T/\sqrt{P}$ plane, Fig. 5 shows that the first-order phase transition line separating the thermal AdS phase and large RNAdS BH exists when $\Phi < \Phi_c = 1$. It is noteworthy that there are two branches of RNAdS black hole solutions for $\Phi < \Phi_c$, and only one branch for $\Phi > \Phi_c$. In the large Φ regime, the large hairy BH phase can be globally stable for some range of $\tilde{T}$, and is bounded by zeroth-order and second-order phase transition lines, which merge at the point S.

We depict phase diagrams in the P-T plane for $\Phi = 0.99382$ and $\Phi = 1.37442$ in Fig. 6. When $\Phi = 0.99382$, the left panel of Fig. 6 displays that the first-order phase transition line is semi-infinite in the P-T plane, which is reminiscent of the solid/liquid phase transition. The zoomed-in inset shows that large hairy BH exists for a narrow range of $\tilde{T}$, and is separated from RNAdS black

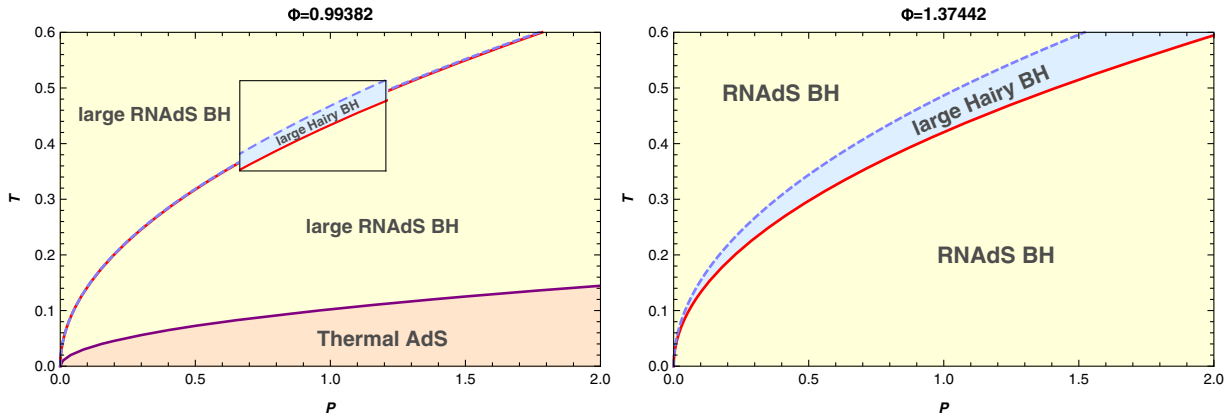

FIG. 6. Phase diagrams of the grand canonical ensemble of hairy and RNAdS black holes with $\alpha = 5$ in the P-T plane. Left panel: $\Phi = 0.99382$. There is a first-order phase transition line (purple line) between the thermal AdS space and large RNAdS BH, which is semi-infinite in the P-T plane and reminiscent of the solid/liquid phase transition. The inset exhibits the large hairy BH phase between the zeroth-order (red line) and second-order (blue dashed line) phase transition lines. Right panel: $\Phi = 1.37442$. The thermal AdS space and the first-order Hawking-Page phase transition are absent. RNAdS black holes have only one phase, namely RNAdS BH. The blue strip, corresponding to large hairy BH, resembles that in the left panel, but with a larger width.

holes by the zeroth-order and second-order phase transition lines. On the other hand, when $\Phi = 1.37442$, the thermal AdS phase is never globally preferred, and RNAdS black hole solutions are always single-valued. So in the right panel of Fig. 6, only RNAdS BH and large hairy BH, as well as the associated zeroth-order and second-order phase transitions, are presented.

B. Canonical ensemble

In a canonical ensemble with fixed black hole charge Q and temperature T, we use the free energy (42) to study phase structure and transitions of RNAdS and hairy black holes. Furthermore, a specific heat at constant charge and pressure,

$$C_{Q,P} = T\left(\frac{\partial S}{\partial T}\right)_{Q,P} = \frac{3\tilde{r}_+\tilde{T}}{4P}\left(\frac{\partial \tilde{r}_+}{\partial \tilde{T}}\right)_{Q,P}, \tag{45}$$

is used to investigate the local thermal stability of black holes in the canonical ensemble.

We plot the reduced horizon radius $\tilde{r}_+$ and the free energy $\tilde{F}$ as functions of reduced temperature $\tilde{T}$ for RNAdS and hairy black holes with three representative values of $\tilde{Q}$ in Fig. 7, where we have $\alpha = 5$. The presence of multi-valued functions $\tilde{r}_+(\tilde{T})$ indicates that black hole solutions can possess multi branches of different horizon radii, which may lead to phase transitions. The lower row exhibits the free energy $\tilde{F}$ against the temperature $\tilde{T}$, which shows globally preferred phases. In the left column, there are three branches of RNAdS black holes in some range of $\tilde{T}$, dubbed large, intermediate and small RNAdS BHs depending on their sizes of horizon radius. Whereas hairy black holes, emerging from the bifurcation point B, have only one branch of solutions. It shows that a first-order phase transition occurs between large and small RNAdS BH phases, both of which have positive $C_{Q,P}$, and hence are thermally stable. In the middle column of Fig. 7, RNAdS and hairy black holes both have a single phase. Moreover, the RNAdS black holes are always globally preferred over the hairy black holes, and therefore there is no phase transitions. In the right column of Fig. 7, there are only one branch of RNAdS black hole solutions and two branches of hairy black hole solutions. The inset displays that, as $\tilde{T}$ increases from 0, the system undergoes a zeroth-order phase transition from RNAdS BH to large hairy BH at $\tilde{T} = \tilde{T}_{\min}$ and a second-order phase transition from large hairy BH to RNAdS BH at the bifurcation point B, corresponding to a RNAdS BH/large hairy BH/RNAdS BH reentrant phase transition. Note that both globally preferred phases are thermally stable with a positive $C_{Q,P}$.

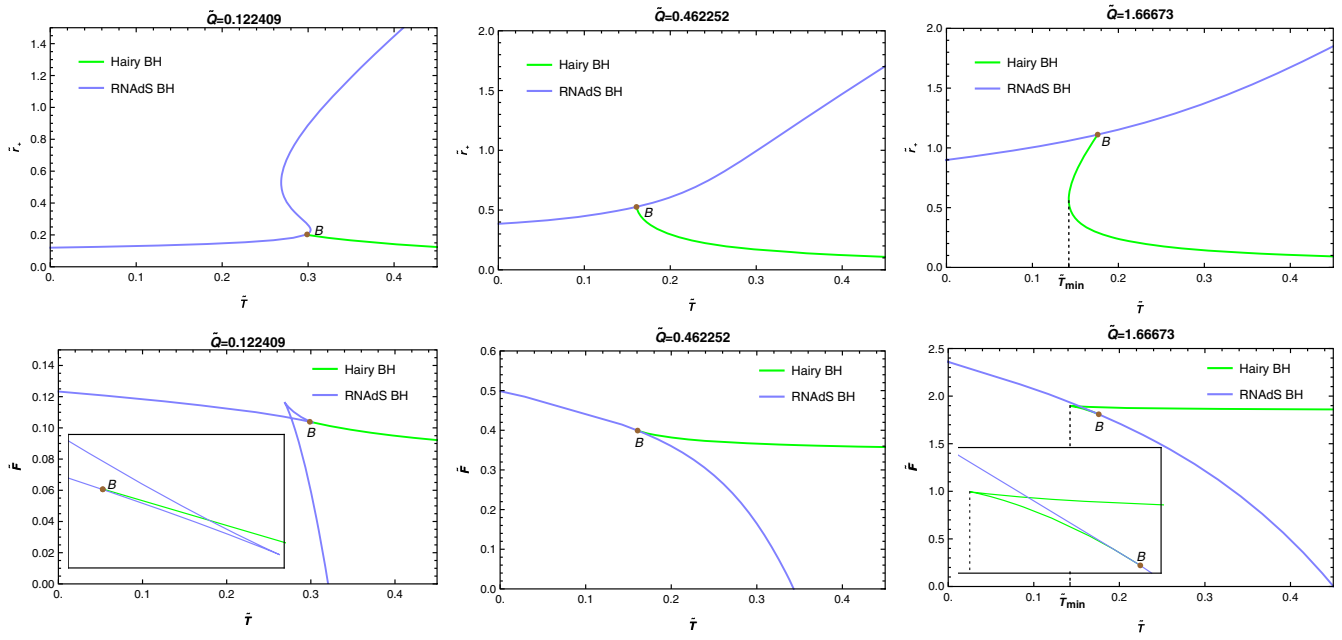

FIG. 7. Plots of the reduced horizon radius $\tilde{r}_+$ (upper row) and the reduced free energy $\tilde{F}$ (lower row) against the reduced temperature $\tilde{T}$ for RNAdS (blue lines) and hairy (green lines) black holes with three values of reduced charge $\tilde{Q}$ in the canonical ensemble. Bifurcation points are marked by B. Left column: $\tilde{Q} = 0.122409$. Three branches of RNAdS black hole solutions coexist in some range of $\tilde{T}$, where a first-order phase transition between large RNAdS BH and small RNAdS BH occurs. Hairy black holes bifurcate from RNAdS black holes at the point B with a higher free energy, and therefore are not the globally preferred phase. Center column: $\tilde{Q} = 0.462252$. There is only one branch for RNAdS and hairy black hole solutions, and no phase transition occurs. Right column: $\tilde{Q} = 1.66673$. RNAdS black holes coexist with two branches of hairy black holes in a certain range of $\tilde{T}$, where large hairy BH is globally preferred. A RNAdS BH/large hairy BH/RNAdS BH reentrant phase transition, consisting of zeroth-order and second-order phase transitions, occurs as $\tilde{T}$ increases.

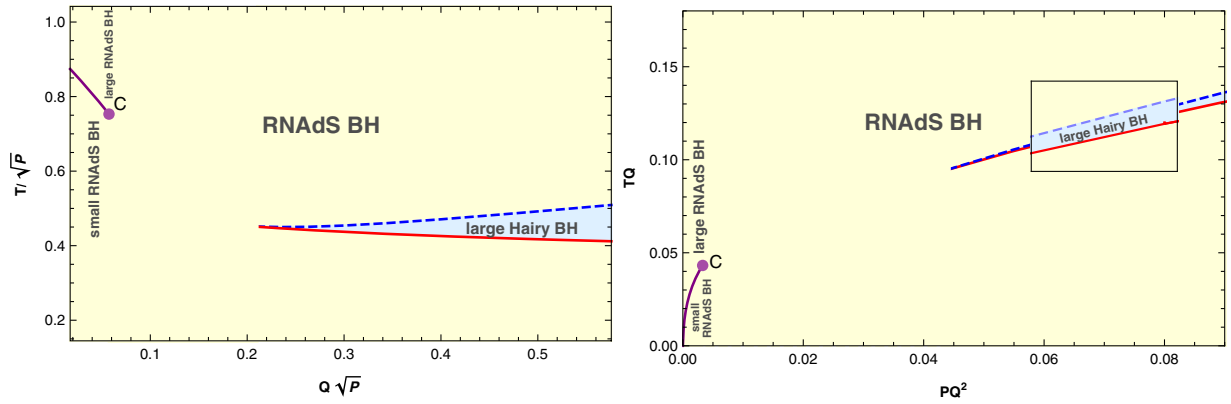

FIG. 8. Phase diagrams of the canonical ensemble of RNAdS and hairy black holes with $\alpha = 5$ in the $Q\sqrt{P}$-$T/\sqrt{P}$ (left panel) and PQ^2-TQ (right panel) planes. There is a first-order phase transition (purple line) between small and large RNAdS BHs, which terminates at a critical point C. Past the critical point, RNAdS black holes have only one phase, and large hairy BH can be the globally stable phase. For a large value of $Q\sqrt{P}$ or PQ^2, the system undergoes a RNAdS BH/large hairy BH/RNAdS reentrant phase transition, which is composed of zeroth-order (red line) and second-order (blue dashed line) phase transitions, with the temperature increasing.

In Fig. 8, the phase diagrams display the globally stable phases with the lowest free energy in the $Q\sqrt{P} - T/\sqrt{P}$ and PQ^2-TQ planes. For a small value of $Q\sqrt{P}$ or PQ^2, a first-order phase transition separates small and large RNAdS BHs and terminates at the critical point, which is reminiscent of the liquid/gas phase transition. However, as $Q\sqrt{P}$ or PQ^2 increases, the large hairy BH phase can be the globally preferred state. In particular, large hairy BH is bounded by second-order and zeroth-order phase transition lines, which corresponds to a RNAdS BH/large hairy BH/RNAdS BH reentrant phase transition.

IV. CONCLUSIONS

In this paper, we first briefly introduced asymptotically AdS hairy black holes in the EMS model [96], where a nonminimal coupling function $f(\phi) = e^{\alpha\phi^2}$ between the scalar and Maxwell fields was considered. We then derived the first law of thermodynamics following the covariant construction associated with the diffeomorphism symmetry, and obtained the Smarr relation by computing a Komar integral with respect to a timelike Killing vector. Focusing on the extended phase space, we found that the conjugate thermodynamic volume of hairy black holes is different from the "naive" geometric volume (i.e., $4\pi r_+^3/3$), and computed the regularized on-shell Euclidean action to obtain the free energy of black holes in canonical and grand canonical ensembles.

In the EMS model, there exists some parameter region where hairy and RNAdS black holes coexist, which leads to complicated phase structure in canonical and grand canonical ensembles. In the grand canonical ensemble, a thermal AdS/large RNAdS BH first-order phase transition occurs for a small Φ, which composes a semi-infinite coexistence line in the P-T diagram and is reminiscent of the solid/liquid phase transition. In the canonical ensemble, there is a small RNAdS BH/large RNAdS BH first-order phase transition, which terminates at a critical point and hence resembles the liquid/gas phase transition. For a large value of $\tilde{Q}/\Phi$ in the canonical/grand canonical ensemble, the hairy BH phase can possess a lower free energy than that of RNAdS BH phases, and thus becomes globally preferred in some range of the temperature. The presence of globally stable hairy BH phases therefore enriches the phase structure, which leads to the existence of reentrant phase transitions between RNAdS and hairy black holes. Specifically, as the temperature monotonically increases, the globally stable phase turns to the hairy black holes from the RNAdS black holes at a zero-order phase transition, and eventually returns to the RNAdS black holes after a second-order phase transition.

As discussed in the Introduction, the reentrant phase transitions that have been reported in the context of black holes usually include zeroth-order and first-order phase transitions. However, the reentrant phase transitions in our paper were found to consist of zeroth-order and second-order phase transitions. It is noteworthy that the second-order phase transition line corresponds to a bifurcation line, at which hairy black holes can be induced from RNAdS black holes. Therefore, the RNAdS BH/hairy BH/RNAdS BH reentrant phase transition could be used to understand the dynamical evolution of hairy black holes from RNAdS ones in the perspective of black hole thermodynamics. Moreover, the second-order phase transition between RNAdS and hairy black holes may provide important holographic applications.

ACKNOWLEDGMENTS

We are grateful to Qingyu Gan and Feiyu Yao for useful discussions and valuable comments. This work is supported in part by NSFC (Grants No. 11875196, No. 11375121, No. 11947225 and No. 11005016).

[1] B. P. Abbott *et al.*, Observation of Gravitational Waves from a Binary Black Hole Merger, Phys. Rev. Lett. **116**, 061102 (2016).

[2] Kazunori Akiyama *et al.*, First M87 Event Horizon Telescope results. I. The shadow of the supermassive black hole, Astrophys. J. Lett. **875**, L1 (2019).

[3] S. W. Hawking, Particle creation by black holes, Commun. Math. Phys. **43**, 199 (1975); **46**, 206(E) (1976).

[4] Jacob D. Bekenstein, Black holes and the second law, Lett. Nuovo Cimento **4**, 737 (1972).

[5] Jacob D. Bekenstein, Black holes and entropy, Phys. Rev. D **7**, 2333 (1973).

[6] James M. Bardeen, B. Carter, and S. W. Hawking, The four laws of black hole mechanics, Commun. Math. Phys. **31**, 161 (1973).

[7] S. W. Hawking and Don N. Page, Thermodynamics of black holes in anti-de Sitter space, Commun. Math. Phys. **87**, 577 (1983).

[8] Juan Martin Maldacena, The large N limit of superconformal field theories and supergravity, Adv. Theor. Math. Phys. **2**, 231 (1998).

[9] S. S. Gubser, I. R. Klebanov, and A. M. Polyakov, Gauge theory correlators from noncritical string theory, Phys. Lett. B **428**, 105 (1998).

[10] Edward Witten, Anti-de Sitter space and holography, Adv. Theor. Math. Phys. **2**, 253 (1998).

[11] Edward Witten, Anti-de Sitter space, thermal phase transition, and confinement in gauge theories, Adv. Theor. Math. Phys. **2**, 505 (1998).

[12] Mirjam Cvetic and Steven S. Gubser, Phases of R charged black holes, spinning branes and strongly coupled gauge theories, J. High Energy Phys. 04 (1999) 024.

[13] Andrew Chamblin, Roberto Emparan, Clifford V. Johnson, and Robert C. Myers, Charged AdS black holes and catastrophic holography, Phys. Rev. D **60**, 064018 (1999).

[14] Andrew Chamblin, Roberto Emparan, Clifford V. Johnson, and Robert C. Myers, Holography, thermodynamics and fluctuations of charged AdS black holes, Phys. Rev. D **60**, 104026 (1999).

[15] Marco M. Caldarelli, Guido Cognola, and Dietmar Klemm, Thermodynamics of Kerr-Newman-AdS black holes and conformal field theories, Classical Quantum Gravity **17**, 399 (2000).

[16] Rong-Gen Cai, Gauss-Bonnet black holes in AdS spaces, Phys. Rev. D **65**, 084014 (2002).

[17] Mirjam Cvetic, Shin'ichi Nojiri, and Sergei D. Odintsov, Black hole thermodynamics and negative entropy in de Sitter and anti-de Sitter Einstein-Gauss-Bonnet gravity, Nucl. Phys. **B628**, 295 (2002).

[18] Shin'ichi Nojiri and Sergei D. Odintsov, Anti-de Sitter black hole thermodynamics in higher derivative gravity and new confining-deconfining phases in dual CFT, Phys. Lett. B **521**, 87 (2001); **542**, 301(E) (2002).

[19] Dumitru Astefanesei, Robert B. Mann, and Raúl Rojas, Hairy black hole chemistry, J. High Energy Phys. 11 (2019) 043.

[20] Claudia S. Peca and Jose P. S. Lemos, Thermodynamics of Reissner-Nordstrom anti-de Sitter black holes in the grand canonical ensemble, Phys. Rev. D **59**, 124007 (1999).

[21] Dumitru Astefanesei, David Choque, Francisco Gómez, and Raúl Rojas, Thermodynamically stable asymptotically flat hairy black holes with a dilaton potential, J. High Energy Phys. 03 (2019) 205.

[22] Dumitru Astefanesei, Jose Luis Blázquez-Salcedo, Francisco Gómez, and Raúl Rojas, Thermodynamically stable asymptotically flat hairy black holes with a dilaton potential: The general case, J. High Energy Phys. 02 (2021) 233.

[23] J. W. York, Jr., Black hole thermodynamics and the Euclidean Einstein action, Phys. Rev. D **33**, 2092 (1986).

[24] Harry W. Braden, J. David Brown, Bernard F. Whiting, and James W. York, Charged black hole in a grand canonical ensemble, Phys. Rev. D **42**, 3376 (1990).

[25] Steven Carlip and S. Vaidya, Phase transitions and critical behavior for charged black holes, Classical Quantum Gravity **20**, 3827 (2003).

[26] Andrew P. Lundgren, Charged black hole in a canonical ensemble, Phys. Rev. D **77**, 044014 (2008).

[27] Peng Wang, Haitang Yang, and Shuxuan Ying, Thermodynamics and phase transition of a Gauss-Bonnet black hole in a cavity, Phys. Rev. D **101**, 064045 (2020).

[28] Peng Wang, Houwen Wu, and Haitang Yang, Thermodynamics and phase transition of a nonlinear electrodynamics black hole in a cavity, J. High Energy Phys. 07 (2019) 002.

[29] Kangkai Liang, Peng Wang, Houwen Wu, and Mingtao Yang, Phase structures and transitions of Born–Infeld black holes in a grand canonical ensemble, Eur. Phys. J. C **80**, 187 (2020).

[30] Peng Wang, Houwen Wu, and Haitang Yang, Thermodynamic geometry of AdS black holes and black holes in a cavity, Eur. Phys. J. C **80**, 216 (2020).

[31] Peng Wang, Houwen Wu, and Shuxuan Ying, Validity of thermodynamic laws and weak cosmic censorship for AdS black holes and black holes in a cavity, Chin. Phys. C **45**, 055105 (2021).

[32] Brian P. Dolan, Pressure and volume in the first law of black hole thermodynamics, Classical Quantum Gravity **28**, 235017 (2011).

[33] David Kubiznak and Robert B. Mann, P-V criticality of charged AdS black holes, J. High Energy Phys. 07 (2012) 033.

[34] David Kubiznak, Robert B. Mann, and Mae Teo, Black hole chemistry: Thermodynamics with Lambda, Classical Quantum Gravity **34**, 063001 (2017).

[35] David Kastor, Sourya Ray, and Jennie Traschen, Enthalpy and the mechanics of AdS black holes, Classical Quantum Gravity **26**, 195011 (2009).

[36] Shao-Wen Wei and Yu-Xiao Liu, Critical phenomena and thermodynamic geometry of charged Gauss-Bonnet AdS black holes, Phys. Rev. D **87**, 044014 (2013).

[37] Sharmila Gunasekaran, Robert B. Mann, and David Kubiznak, Extended phase space thermodynamics for charged and rotating black holes and Born-Infeld vacuum polarization, J. High Energy Phys. 11 (2012) 110.

[38] Rong-Gen Cai, Li-Ming Cao, Li Li, and Run-Qiu Yang, P-V criticality in the extended phase space of Gauss-Bonnet black holes in AdS space, J. High Energy Phys. 09 (2013) 005.

[39] Wei Xu and Liu Zhao, Critical phenomena of static charged AdS black holes in conformal gravity, Phys. Lett. B **736**, 214 (2014).
[40] Antonia M. Frassino, David Kubiznak, Robert B. Mann, and Fil Simovic, Multiple reentrant phase transitions and triple points in Lovelock thermodynamics, J. High Energy Phys. 09 (2014) 080.
[41] M. H. Dehghani, S. Kamrani, and A. Sheykhi, $P-V$ criticality of charged dilatonic black holes, Phys. Rev. D **90**, 104020 (2014).
[42] Robie A. Hennigar, Wilson G. Brenna, and Robert B. Mann, $P-v$ criticality in quasitopological gravity, J. High Energy Phys. 07 (2015) 077.
[43] Elena Caceres, Phuc H. Nguyen, and Juan F. Pedraza, Holographic entanglement entropy and the extended phase structure of STU black holes, J. High Energy Phys. 09 (2015) 184.
[44] Shao-Wen Wei and Yu-Xiao Liu, Insight into the Microscopic Structure of an AdS Black Hole from a Thermodynamical Phase Transition, Phys. Rev. Lett. **115**, 111302 (2015); **116**, 169903(E) (2016).
[45] Seyed Hossein Hendi, Gu-Qiang Li, Jie-Xiong Mo, Shahram Panahiyan, and Behzad Eslam Panah, New perspective for black hole thermodynamics in Gauss-Bonnet-Born-Infeld massive gravity, Eur. Phys. J. C **76**, 571 (2016).
[46] S. H. Hendi, R. B. Mann, S. Panahiyan, and B. Eslam Panah, Van der Waals like behavior of topological AdS black holes in massive gravity, Phys. Rev. D **95**, 021501 (2017).
[47] José P. S. Lemos and Oleg B. Zaslavskii, Black hole thermodynamics with the cosmological constant as independent variable: Bridge between the enthalpy and the Euclidean path integral approaches, Phys. Lett. B **786**, 296 (2018).
[48] Juan F. Pedraza, Watse Sybesma, and Manus R. Visser, Hyperscaling violating black holes with spherical and hyperbolic horizons, Classical Quantum Gravity **36**, 054002 (2019).
[49] Peng Wang, Houwen Wu, and Haitang Yang, Thermodynamics and phase transitions of nonlinear electrodynamics black holes in an extended phase space, J. Cosmol. Astropart. Phys. 04 (2019) 052.
[50] Shao-Wen Wei, Yu-Xiao Liu, and Robert B. Mann, Repulsive Interactions and Universal Properties of Charged Anti-de Sitter Black Hole Microstructures, Phys. Rev. Lett. **123**, 071103 (2019).
[51] Shao-Wen Wei and Yu-Xiao Liu, Extended thermodynamics and microstructures of four-dimensional charged Gauss-Bonnet black hole in AdS space, Phys. Rev. D **101**, 104018 (2020).
[52] David Kubiznak and Robert B. Mann, Black hole chemistry, Can. J. Phys. **93**, 999 (2015).
[53] Natacha Altamirano, David Kubiznak, and Robert B. Mann, Reentrant phase transitions in rotating anti-de Sitter black holes, Phys. Rev. D **88**, 101502 (2013).
[54] De-Cheng Zou, Ruihong Yue, and Ming Zhang, Reentrant phase transitions of higher-dimensional AdS black holes in dRGT massive gravity, Eur. Phys. J. C **77**, 256 (2017).
[55] Robie A. Hennigar and Robert B. Mann, Reentrant phase transitions and van der Waals behaviour for hairy black holes, Entropy **17**, 8056 (2015).
[56] Claude Silbert Hudson, Die gegenseitige löslichkeit von nikotin in wasser, Z. Phys. Chem. (Leipzig) **47**, 113 (1904).
[57] Andreas Karch and Brandon Robinson, Holographic black hole chemistry, J. High Energy Phys. 12 (2015) 073.
[58] Abdulrahim Al Balushi, Robie A. Hennigar, Hari K. Kunduri, and Robert B. Mann, Holographic Complexity and Thermodynamic Volume, Phys. Rev. Lett. **126**, 101601 (2021).
[59] Wan Cong, David Kubiznak, and Robert B. Mann, Thermodynamics of AdS Black Holes: Central Charge Criticality, Phys. Rev. Lett. **127**, 091301 (2021).
[60] Fil Simovic and Robert B. Mann, Critical phenomena of charged de Sitter black Holes in cavities, Classical Quantum Gravity **36**, 014002 (2019).
[61] Peng Wang, Houwen Wu, Haitang Yang, and Feiyu Yao, Extended phase space thermodynamics for black holes in a cavity, J. High Energy Phys. 09 (2020) 154.
[62] Werner Israel, Event horizons in static vacuum spacetimes, Phys. Rev. **164**, 1776 (1967).
[63] B. Carter, Axisymmetric Black Hole has Only Two Degrees of Freedom, Phys. Rev. Lett. **26**, 331 (1971).
[64] Remo Ruffini and John A. Wheeler, Introducing the black hole, Phys. Today **24**, No. 1, 30 (1971).
[65] M. S. Volkov and D. V. Galtsov, NonAbelian Einstein Yang-Mills black holes, JETP Lett. **50**, 346 (1989).
[66] P. Bizon, Colored Black Holes, Phys. Rev. Lett. **64**, 2844 (1990).
[67] Brian R. Greene, Samir D. Mathur, and Christopher M. O'Neill, Eluding the no hair conjecture: Black holes in spontaneously broken gauge theories, Phys. Rev. D **47**, 2242 (1993).
[68] Hugh Luckock and Ian Moss, Black holes have skyrmion hair, Phys. Lett. B **176**, 341 (1986).
[69] Serge Droz, Markus Heusler, and Norbert Straumann, New black hole solutions with hair, Phys. Lett. B **268**, 371 (1991).
[70] P. Kanti, N. E. Mavromatos, J. Rizos, K. Tamvakis, and E. Winstanley, Dilatonic black holes in higher curvature string gravity, Phys. Rev. D **54**, 5049 (1996).
[71] Subhash Mahapatra, Supragyan Priyadarshinee, Gosala Narasimha Reddy, and Bhaskar Shukla, Exact topological charged hairy black holes in AdS Space in D-dimensions, Phys. Rev. D **102**, 024042 (2020).
[72] Carlos A. R. Herdeiro and Eugen Radu, Asymptotically flat black holes with scalar hair: A review, Int. J. Mod. Phys. D **24**, 1542014 (2015).
[73] Carlos A. R. Herdeiro, Eugen Radu, Nicolas Sanchis-Gual, and José A. Font, Spontaneous Scalarization of Charged Black Holes, Phys. Rev. Lett. **121**, 101102 (2018).
[74] Pedro G. S. Fernandes, Carlos A. R. Herdeiro, Alexandre M. Pombo, Eugen Radu, and Nicolas Sanchis-Gual, Spontaneous scalarisation of charged black holes: Coupling dependence and dynamical features, Classical Quantum Gravity **36**, 134002 (2019); **37**, 049501(E) (2020).
[75] Jose Luis Blázquez-Salcedo, Carlos A. R. Herdeiro, Jutta Kunz, Alexandre M. Pombo, and Eugen Radu,

Einstein-Maxwell-scalar black holes: The hot, the cold and the bald, Phys. Lett. B **806**, 135493 (2020).
[76] D. Astefanesei, C. Herdeiro, A. Pombo, and E. Radu, Einstein-Maxwell-scalar black holes: Classes of solutions, dyons and extremality, J. High Energy Phys. 10 (2019) 078.
[77] Pedro G. S. Fernandes, Carlos A. R. Herdeiro, Alexandre M. Pombo, Eugen Radu, and Nicolas Sanchis-Gual, Charged black holes with axionic-type couplings: Classes of solutions and dynamical scalarization, Phys. Rev. D **100**, 084045 (2019).
[78] De-Cheng Zou and Yun Soo Myung, Scalarized charged black holes with scalar mass term, Phys. Rev. D **100**, 124055 (2019).
[79] Pedro G. S. Fernandes, Einstein-Maxwell-scalar black holes with massive and self-interacting scalar hair, Phys. Dark Universe **30**, 100716 (2020).
[80] Yan Peng, Scalarization of horizonless reflecting stars: Neutral scalar fields non-minimally coupled to Maxwell fields, Phys. Lett. B **804**, 135372 (2020).
[81] Yun Soo Myung and De-Cheng Zou, Instability of Reissner–Nordström black hole in Einstein-Maxwell-scalar theory, Eur. Phys. J. C **79**, 273 (2019).
[82] Yun Soo Myung and De-Cheng Zou, Stability of scalarized charged black holes in the Einstein–Maxwell–Scalar theory, Eur. Phys. J. C **79**, 641 (2019).
[83] De-Cheng Zou and Yun Soo Myung, Radial perturbations of the scalarized black holes in Einstein-Maxwell-conformally coupled scalar theory, Phys. Rev. D **102**, 064011 (2020).
[84] Yun Soo Myung and De-Cheng Zou, Onset of rotating scalarized black holes in Einstein-Chern-Simons-Scalar theory, Phys. Lett. B **814**, 136081 (2021).
[85] Zhan-Feng Mai and Run-Qiu Yang, Stability analysis on charged black hole with non-linear complex scalar, Phys. Rev. D **104**, 044008 (2021).
[86] Dumitru Astefanesei, Carlos Herdeiro, João Oliveira, and Eugen Radu, Higher dimensional black hole scalarization, J. High Energy Phys. 09 (2020) 186.
[87] Yun Soo Myung and De-Cheng Zou, Quasinormal modes of scalarized black holes in the Einstein-Maxwell-scalar theory, Phys. Lett. B **790**, 400 (2019).
[88] Jose Luis Blázquez-Salcedo, Carlos A. R. Herdeiro, Sarah Kahlen, Jutta Kunz, Alexandre M. Pombo, and Eugen Radu, Quasinormal modes of hot, cold and bald Einstein-Maxwell-scalar black holes, Eur. Phys. J. C **81**, 155 (2021).
[89] Yun Soo Myung and De-Cheng Zou, Scalarized charged black holes in the Einstein-Maxwell-Scalar theory with two U(1) fields, Phys. Lett. B **811**, 135905 (2020).
[90] Yun Soo Myung and De-Cheng Zou, Scalarized black holes in the Einstein-Maxwell-scalar theory with a quasi-topological term, Phys. Rev. D **103**, 024010 (2021).
[91] Hong Guo, Xiao-Mei Kuang, Eleftherios Papantonopoulos, and Bin Wang, Topology and spacetime structure influences on black hole scalarization, Eur. Phys. J. C **81**, 842 (2021).
[92] Peng Wang, Houwen Wu, and Haitang Yang, Scalarized Einstein-Born-Infeld black holes, Phys. Rev. D **103**, 104012 (2021).
[93] Cheng-Yong Zhang, Peng Liu, Yunqi Liu, Chao Niu, and Bin Wang, Dynamical charged black hole spontaneous scalarization in anti-de Sitter spacetimes, Phys. Rev. D **104**, 084089 (2021).
[94] Qingyu Gan, Peng Wang, Houwen Wu, and Haitang Yang, Photon spheres and spherical accretion image of a hairy black hole, Phys. Rev. D **104**, 024003 (2021).
[95] Qingyu Gan, Peng Wang, Houwen Wu, and Haitang Yang, Photon ring and observational appearance of a hairy black hole, Phys. Rev. D **104**, 044049 (2021).
[96] Guangzhou Guo, Peng Wang, Houwen Wu, and Haitang Yang, Scalarized Einstein-Maxwell-scalar black holes in anti-de Sitter spacetime, Eur. Phys. J. C **81**, 864 (2021).
[97] Christopher P. Herzog, Lectures on holographic superfluidity and superconductivity, J. Phys. A **42**, 343001 (2009).
[98] Gary T. Horowitz, Introduction to holographic superconductors, Lect. Notes Phys. **828**, 313 (2011).
[99] Nami Uchikata and Shijun Yoshida, Quasinormal modes of a massless charged scalar field on a small Reissner-Nordström-anti-de Sitter black hole, Phys. Rev. D **83**, 064020 (2011).
[100] Sean A. Hartnoll, Christopher P. Herzog, and Gary T. Horowitz, Building a Holographic Superconductor, Phys. Rev. Lett. **101**, 031601 (2008).
[101] C. P. Herzog, P. K. Kovtun, and D. T. Son, Holographic model of superfluidity, Phys. Rev. D **79**, 066002 (2009).
[102] J. Lee and Robert M. Wald, Local symmetries and constraints, J. Math. Phys. (N.Y.) **31**, 725 (1990).
[103] Robert M. Wald, Black hole entropy is the Noether charge, Phys. Rev. D **48**, R3427(R) (1993).
[104] Vivek Iyer and Robert M. Wald, Some properties of Noether charge and a proposal for dynamical black hole entropy, Phys. Rev. D **50**, 846 (1994).
[105] Miho Urano, Akira Tomimatsu, and Hiromi Saida, Mechanical first law of black hole spacetimes with cosmological constant and its application to Schwarzschild-de Sitter spacetime, Classical Quantum Gravity **26**, 105010 (2009).
[106] Shao-Feng Wu, Xian-Hui Ge, and Yu-Xiao Liu, First law of black hole mechanics in variable background fields, Gen. Relativ. Gravit. **49**, 85 (2017).
[107] M. Cvetic, G. W. Gibbons, D. Kubiznak, and C. N. Pope, Black hole enthalpy and an entropy inequality for the thermodynamic volume, Phys. Rev. D **84**, 024037 (2011).
[108] Robie A. Hennigar, David Kubizňák, and Robert B. Mann, Entropy Inequality Violations from Ultraspinning Black Holes, Phys. Rev. Lett. **115**, 031101 (2015).
[109] Dietmar Klemm, Four-dimensional black holes with unusual horizons, Phys. Rev. D **89**, 084007 (2014).
[110] Robie A. Hennigar, David Kubizňák, Robert B. Mann, and Nathan Musoke, Ultraspinning limits and super-entropic black holes, J. High Energy Phys. 06 (2015) 096.
[111] Hongmei Jing, Benrong Mu, Jun Tao, and Peng Wang, Thermodynamic instability of 3D Einstein-Born-Infeld AdS black holes, Chin. Phys. C **45**, 065103 (2021).
[112] Larry Smarr, Mass Formula for Kerr Black Holes, Phys. Rev. Lett. **30**, 71 (1973); **30**, 521(E) (1973).
[113] Roberto Emparan, Clifford V. Johnson, and Robert C. Myers, Surface terms as counterterms in the AdS/CFT correspondence, Phys. Rev. D **60**, 104001 (1999).

[114] Vijay Balasubramanian and Per Kraus, A stress tensor for anti-de Sitter gravity, Commun. Math. Phys. **208**, 413 (1999).
[115] Rodrigo Olea, Mass, angular momentum and thermodynamics in four-dimensional Kerr-AdS black holes, J. High Energy Phys. 06 (2005) 023.
[116] Rodrigo Olea, Regularization of odd-dimensional AdS gravity: Kounterterms, J. High Energy Phys. 04 (2007) 073.
[117] Olivera Miskovic and Rodrigo Olea, Thermodynamics of Einstein-Born-Infeld black holes with negative cosmological constant, Phys. Rev. D **77**, 124048 (2008).
[118] Bom Soo Kim, Holographic renormalization of Einstein-Maxwell-dilaton theories, J. High Energy Phys. 11 (2016) 044.